受入
86-11-116
高工研図書室

EUROPEAN ORGANIZATION FOR NUCLEAR RESEARCH

CERN/EP 86-166
21 October 1986

NEUTRAL STRANGE PARTICLE CORRELATIONS IN 360 GeV/c pp INTERACTIONS

EHS-RCBC Collaboration

Bombay[1]-Budapest[2]-CERN[3]-Chandigarh[4]-Genova[5]-Innsbruck[6]-Japan-UG[7]-Madrid[8]-Mons[9]-Moscow[10]-Rutgers[11]-Serpukhov[12]-Tennessee[13]-Vienna[14] Collaboration

M. Asai[7d], T. Aziz[1], J.L. Bailly[9], J.F. Baland[9], S. Banerjee[1], W. Bartl[14], A. Batunin[12], C. Caso[5], F. Diez-Medo[8], B. Epp[6], A. Ferrando[8], F. Fontanelli[5], S.N. Ganguli[1], V.G. Gavrjusev[10], T. Gemesy[2], P. Girtler[6], A. Gurtu[1], R. Hamatsu[7a], P. Herquet[9], Y. Iga[7a], E. Kistenev[12], J.M. Kohli[4], J. Mac Naughton[14], J.C. Marin[3], M. Markytan[14], L. Montanet[3], G. Neuhofer[3], G. Pinter[2], P. Porth[14], R. Raghavan[1], T. Rodrigo[8], J.M. Salicio[8], J.B. Singh[4], S. Squarcia[5], K. Takahashi[7b], L.A. Tikhonova[10], U. Trevisan[5], T. Tsurugai[7a], V. Yarba[12], G. Zholobov[12] and S. Zotkin[10]

1 Tata Institute of Fundamental Research, 400005 Bombay, India
2 Central Research Institute for Physics, H-1525 Budapest 114, Hungary
3 CERN, European Organization for Nuclear Research, CH-1211 Geneva 23, Switzerland
4 Panjab University, 160014 Chandigarh, India
5 University of Genova and INFN, I-16146 Genova, Italy
6 Institut für Experimentalphysik, A-6020 Innsbruck, Austria(*)
7a Tokyo Metropolitan University, 158 Tokyo, Japan
7b Tokyo University of Agriculture and Technology, Tokyo, Japan
7c Chuo University, Tokyo, Japan
7d Hiroshima University, 730 Hiroshima, Japan
8 Junta de Energia Nuclear, Madrid 3, Spain
9 Université de l'Etat, Faculté des Sciences, B-7000 Mons, Belgium
10 Moscow State University, SU-117234 Moscow, USSR
11 Rutgers University, New Brunswick, NJ08903, USA
12 Institute for High Energy Physics, Serpukhov, SU-142284 Protvino, USSR
13 University of Tennessee, Knoxville, TN 37916, USA
14 Institut für Hochenergiephysik, A-1050 Wien, Austria(*)

Submitted to Zeitschrift für Physik C

(*) Supported by: Fonds zur Förderung der Wissenschaftliche Forschung.

EP/3216P/PP/ed

ABSTRACT

Production properties and correlations for $K^0_s K^0_s$, $K^0_s \Lambda$, $K^0_s \bar{\Lambda}$ and $\Lambda\bar{\Lambda}$ systems in 360 GeV/c pp interactions are presented. All rapidity gap distributions are observed to peak at $\Delta y = 0$ and the azimuthal angular distributions between the two particles are consistent with being flat. Experimental results are compared with the quark fusion and Lund models of particle production.

1. INTRODUCTION

In recent years the quark parton picture has been applied to low p_T hadronic interactions to explain the general features of the observed inclusive distributions [1-11]. Within the general framework of quantum chromodynamics there are two distinguishable mechanisms characterizing the initial state interaction of the colliding hadrons, (a) vector gluon exchange, (b) quark exchange or annihilation. Besides that one may have several non-perturbative corrections via fragmentation or recombinations. Single particle distributions can be described fairly well by a variety of models [12]. Hard processes in hadronic collisions, particularly heavy flavour production, have been tried to be understood by quark-antiquark/ gluon-gluon fusion or flavour excitation models [13-20]. In all these models the crucial test lies in the predictions for correlation parameters [21-22].

In this paper, we present an inclusive study of V^o pairs in pp interactions at 360 GeV/c. Since there are no strange valence quarks in the initial state, the strangeness label might help in revealing the underlying dynamics. So far there exist very little data on strange particle correlations [23-26] in hadronic collisions.

The paper is organised as follows: experimental details are given in sect. 2. Models used for comparison with data are mentioned in sect. 3. Results on $K^o_s K^o_s$ correlation are discussed in sect. 4. Sects 5 and 6 contain results on $K^o_s\Lambda$ and $K^o_s\bar{\Lambda}/\Lambda\bar{\Lambda}$ correlations respectively. We have summarized the results in sect. 7.

2. EXPERIMENTAL DETAILS

The present data come from the experiment NA23 performed at CERN using the European Hybrid Spectrometer (EHS) equipped with a Rapid Cycling Bubble Chamber (RCBC). The set up was exposed to a 360 GeV/c proton beam from the SPS. The relevant details regarding the set up, beam, exposure, data processing, etc. have been published earlier [27-29]. The data sample corresponds to a sensitivity of 1.6 events/μb.

The present data sample contains a total of 194 pairs of V°'s, i.e. neutral strange particles. However, a considerable fraction of the V°'s give rise to ambiguous fits to K^o_s, Λ or $\bar{\Lambda}$ hypotheses.

Keeping only the hypotheses with a kinematic probability larger than 2%, introducing a fiducial volume to guarantee a good momentum determination and imposing a minimum decay length of 3 cm, the sample with ambiguous solutions reduces to 12%. All remaining ambiguities are resolved by using cuts on p_T of the decay products and their effective masses. For example in resolving a K^o/Λ or $K^o/\bar{\Lambda}$ ambiguity, we chose the $\Lambda/\bar{\Lambda}$ hypothesis if the daughter $p_T < 110$ MeV/c and the measured V° mass (for the $\Lambda/\bar{\Lambda}$ hypothesis) lies between 1.105-1.126 GeV/c^2 (for detail see [30]). This procedure leaves 94 pairs of $K^o_sK^o_s$, 75 pairs of $K^o_s\Lambda$, 14 pairs of $K^o_s\bar{\Lambda}$ and 11 pairs of $\Lambda\bar{\Lambda}$.

As it has been mentioned in an earlier paper [29], the loss of the forward V°'s in the overall c.m. system cannot be compensated by incorporating only the momentum dependent visibility weight. In order to obtain the total inclusive 2 V° cross section, each sample is divided into three categories: (a) both the V°'s in the backward hemisphere; (b) one backward, the other forward; (c) both in the forward hemisphere. From the symmetry of the pp system, we expect the contributions from categories (a) and (c) to be equal. So we ignore all the events in category (c) and correct for them by doubling the sample (a). The correction for losses in category (b) was done by using the ratio of weighted inclusive single V° events in the backward and the forward hemisphere.

3. MODELS USED FOR COMPARISON WITH DATA

3.1 Quark Fusion model

We have followed the prescription that Kniazev et al. [9] used for inclusive single K^o_s production assuming that a strange meson is produced from the fusion of a quark from one hadron with an antiquark from the other hadron. We have generalized this to the case of $K^o_sK^o_s$ production by assuming independent production of the two K^o_s's, i.e., due to fusion of two distinct quark-antiquark pairs. The colliding partons have been treated as massless, their longitudinal momenta described by their respective structure functions [31] and their transverse momenta assumed

to follow a gaussian distribution with $\langle k_T \rangle$ = 0.2 GeV/c. The expression for the double inclusive cross section finally obtained is

$$E_a E_b \frac{d\sigma}{d^3p_a d^3p_b} = \frac{1}{\sigma} E_a \frac{d\sigma}{d^3p_a} \cdot E_b \frac{d\sigma}{d^3p_b}$$

$$= \frac{4C^2}{\sigma} \int F' \cdot J' \cdot k_{T2}\, k_{T4}\, dk_{T2}\, d\phi_2\, dk_{T4}\, d\phi_4 \qquad (1a)$$

with

$$F' = \{F_{1/A}(x_1)\, F_{2/B}(x_2)\, f_1(k_{T1})\, f_2(k_{T2})\}.$$

$$\{F_{3/A}(x_3)\, F_{4/B}(x_4)\, f_3(k_{T3})\, f_4(k_{T4})\} \qquad (1b)$$

and

$$J' = \frac{1}{\sqrt{s}\, E_a x_2 + 2p_{az}E_2} \cdot \frac{1}{\sqrt{s}\, E_b x_4 + 2p_{bz}E_4} \qquad (1c)$$

The subscripts A, B refer to the two protons, a, b refer to the two K^o_s and 1, 2, 3, 4 refer to the partons which fuse to produce the K^o_s's (1 + 2 → a, 3 + 4 → b). Functions F(x) are the appropriate structure functions [31] and $f(k_T)$ are the transverse momentum distributions of the partons, normalized to unity. The incident beam direction is taken as the z axis and the x axis is defined along the transverse momentum vector of the hadron a. Following Kniazev [9],

$$C = \frac{2\pi^2}{3} (2J + 1) \frac{g^2}{4\pi} \qquad (2)$$

where J is the spin of the meson and $g^2/4\pi$ is the strong coupling constant. All relevant distributions can be obtained by appropriate integration of eq. (1a).

3.2 Lund Fragmentation Model

In addition to the quark fusion model we have also compared our results with predictions of the string fragmentation Lund model [32]. The default values of parameters have been used. Individual events have been generated and undergone to the same experimental selections and cuts as the real events. The number of events generated was normalized to the pp inelastic cross section at this energy.

4. RESULTS ON $K^o_s K^o_s$ CORRELATION

4.1 Inclusive cross section

We have observed a total of 94 $K^o_s K^o_s$ pairs out of which 53 have both the K^o_s's emitted in the backward hemisphere. These 53 pairs correspond to a cross section of (0.48 ± 0.07) mb. Using the procedure as described in sect. 2, the total inclusive $K^o_s K^o_s$ cross section is determined to be (1.74 ± 0.18)mb and it has been plotted in fig. 1(a) as a function of the laboratory momentum along with data at other energies [33-37]. We find the cross section to be increasing with c.m. energy and this dependence seems to be similar to that of inclusive K^o_s cross section. The cross section ratio $\sigma(K^o_s K^o_s)/\sigma(K^o_s)$ as a function of incident momentum is shown in fig. 1(b). If all kaons are produced as $K\bar{K}$ pairs and if one naively assumes $\sigma(K^+K^-) = \sigma(K^+\bar{K}^o) = \sigma(K^oK^-) = \sigma(K^o\bar{K}^o)$, the cross section ratio is expected to be 1/8. However the observed ratio seems to be larger than 1/8 and as it will be seen later a large fraction of the observed K^o_s is produced with associated Λ.

4.2 Contribution of $K^*(890)$

Fig. 2 shows the semi-inclusive effective mass distribution of $K^o_s\pi^\pm$ from events with $K^o_s K^o_s$. There is an enhancement at a mass around 0.85-0.95 GeV/c^2. To estimate the contribution of $K^*(890)$, the $K^o_s\pi^\pm$ mass distribution is fitted using

$$\frac{dN}{dM_{K\pi}} = BG_{K\pi}(M_{K\pi})[1 + \beta \cdot BW_{K^*}(M_{K\pi})] \tag{3}$$

where $BW_{K^*}(M_{K\pi})$ is the relativistic P-wave Breit-Wigner distribution given by

$$BW_{K^*}(M_{K\pi}) = \frac{M_{K\pi} \cdot M_{K^*} \cdot \Gamma_{K^*}(M_{K\pi})}{(M^2_{K\pi} - M^2_{K^*})^2 + M^2_{K^*}\,\Gamma^2_{K^*}(M_{K\pi})} \tag{4}$$

with

$$\Gamma_{K^*}(M_{K\pi}) = \Gamma_{K^*}\left[\frac{q_{K\pi}}{q_{K^*}}\right]^3 \frac{2q^2_{K^*}}{q^2_{K\pi} + q^2_{K^*}} \tag{5}$$

$M_{K\pi}$ = effective mass of $K^o_s\pi^\pm$ system

M_{K^*}, Γ_{K^*} = mass and width of $K^*(890)$

q_M = momentum of the decay product in the rest frame of invariant mass M

and the background term $BG_{K\pi}(M_{K\pi})$ is parametrized by

$$BG_{K\pi}(M_{K\pi}) = \alpha_1(M_{K\pi} - M_K - M_\pi)^{\alpha_2} \exp(-\alpha_3 M_{K\pi} - \alpha_4 M_{K\pi}^2) \qquad (6)$$

The mass and width of $K^*(890)$ have been kept fixed in the fit using the values given in the PDG table [38]. The fitted result is shown by the solid curve in fig. 2. The contributions of the background and the resonance are shown by the dash-dotted and the dashed curves respectively on the same figure. From the fit and taking into account the $K^{*\pm}$ decay mode into charged kaons, one obtains the cross section of inclusive $K^{*\pm}(890)K_s^o$ production to be (2.0 ± 0.4) mb.

Figs 3(a) and 3(b) show respectively the $K_s^o\pi^-$ and $K_s^o\pi^+$ effective mass distributions when the other $K_s^o\pi^+(K_s^o\pi^-)$ mass falls in the K^* region (between 0.8 and 1.0 GeV/c^2). Fits similar to those described above have been made to these distributions and the results are shown as smooth curves on the figures. The fits lead to the evaluation of $K^{*\pm}K^{*\mp}$ cross section of (0.80 ± 0.25) mb. Thus (28 ± 8)% of the $K_s^oK_s^o$ sample comes from single $K^{*\pm}$ production and (5 ± 1)% of the sample is due to double $K^{*\pm}$ production.

4.3 Kinematic Distributions of $K_s^oK_s^o$ Sample

Fig. 4(a) contains the normalized distribution of the Feynman x variable of the two K_s^o system which shows a sharp fall off at large x-values. A fit of the form

$$\frac{1}{N}\frac{dN}{dx} = A(1 - x)^n \qquad (7)$$

yields A = 9.1 ± 1.5 and n = 8.9 ± 1.0. Fig. 4(b) shows the normalized p_T^2 distribution which exhibits an approximate exponential shape. A fit to

$$\frac{1}{N}\frac{dN}{dp_T^2} = a \exp(-bp_T^2) \qquad (8)$$

gives $a = (2.3 \pm 0.3)(GeV/c)^{-2}$ and $b = (3.2 \pm 0.3)(GeV/c)^{-2}$. Fig. 4(c) shows the two K^o's effective mass distribution. There is an accumulation of events just above the threshold which is often referred to as S^*.

4.4 Longitudinal Correlation

Fig. 5(a) shows the distribution of the rapidity difference between the two K_s^o's (solid circles), $\Delta y = |y_1 - y_2|$. The distribution peaks at 0.0 and the average rapidity gap is 1.1 ± 0.1. This average has to be compared with a value of 1.37 given by a fully randomized technique of merging one K_s^o from one event with another K_s^o belonging to a different event. This clearly indicates that the two K_s^o's are produced in the same rapidity range with a certain degree of positive correlation. If one restricts both the K_s^o's to be in the backward hemisphere (open circles in fig. 5(a)), $\langle\Delta y\rangle$ = 0.70 ± 0.07. The full curves on fig. 5(a) are the predictions of the quark fusion model and the dotted curves are the predictions of the Lund model. The fusion model predicts a sharper enhancement at $\Delta y = 0$ compared to the Lund model, but within experimental errors both models agree reasonably well with the data.

We have also studied the gap length distribution for the Feynman x variable and the results are shown in fig. 5(b). As in the rapidity gap plot there is a peak at $\Delta x = 0$ and the average gap lengths, $\langle\Delta x\rangle$, are 0.09 ± 0.01 for the entire sample and 0.07 ± 0.01 for the sample in which both K_s^o are in the backward hemisphere. Predictions of both models are also shown in the figure. The quark fusion model predicts a very sharp peak at $\Delta x = 0$ with a rapid fall off. The data appear to follow the predictions of the Lund model somewhat better.

4.5 Transverse Correlation

The distribution in the azimuthal correlation angle $\Delta\phi$ (i.e., the angle between the transverse momenta of the two K_s^o's) is shown by the solid circles in fig. 6(a). The average value of the azimuthal correlation angle is found to be $\langle\Delta\phi\rangle$ = (83.4 ± 5.9)degrees. The open circles in fig. 6(a) show similar distribution when both the K_s^o's are emitted in the backward hemisphere. This distribution is consistent with isotropy with $\langle\Delta\phi\rangle$ = (85.1 ± 7.6)degrees. The curves in the figure represent the quark fusion model calculation and the Lund model predictions. Within the present statistics both models agree with the data.

Fig. 6(b) shows the distribution of the ratio of the p_T's of the two K_s^o's, p_{T_1}/p_{T_2} with $p_{T_1} \leq p_{T_2}$. One finds the distribution to be rather smooth with an average value of 0.56 ± 0.03. The open circles in fig. 6(b)

show similar distribution with both K^o_s's in the backward hemisphere. The two distributions (solid and open circles) are rather similar and the average value of p_{T_1}/p_{T_2} of the subsample is 0.57 ± 0.03. Predictions of both fusion and Lund models are almost indistinguishable for this figure and only one set of curves is presented. There is good agreement with data.

5. RESULTS ON K^o_s–Λ CORRELATION

We have observed 75 pairs of $K^o_s\Lambda$ events, out of which 57 pairs correspond to both K^o_s and Λ emitted in the backward hemisphere. After appropriate corrections we obtain cross section of (1.48 ± 0.17) mb for inclusive $K^o_s\Lambda$ sample and (0.45 ± 0.06) mb for both K^o_s and Λ being emitted in the backward hemisphere. Fig. 7 shows the plot of inclusive $K^o_s\Lambda$ cross section as a function of beam momentum [33–37]. One sees the inclusive cross section increasing with c.m. energy.

Fig. 8(a) shows the normalized distribution of the Feynman x variable of $K^o_s\Lambda$ system. The distribution is rather flat as can also be seen from the results of the fit to eq. (7) which yields A = 2.3 ± 0.7 and n = 1.5 ± 0.9. The normalized p_T^2 distribution of the $K^o_s\Lambda$ system is shown in fig. 8(b). The p_T^2 distribution shows an exponential fall off and a fit to eq. (8) gives a = (2.5 ± 0.5)$(GeV/c)^{-2}$ and b = (3.2 ± 0.5)$(GeV/c)^{-2}$. Fig. 8(c) shows the effective mass distribution of $K^o_s\Lambda$ system. The bulk of the data is accumulated below $M_{K^o_s\Lambda}$ of 2 GeV/c^2.

The radidity gap distribution of the $K_s\Lambda$ sample in which both are in the backward hemisphere is shown in fig. 9(a). The histogram peaks at $\Delta y = 0$; the average rapidity gap is $\langle\Delta y\rangle = 0.96 \pm 0.10$. Fig. 9(b) shows the Feynman x gap distribution; the average gap is $\langle\Delta x\rangle = 0.21 \pm 0.02$. Lund model predictions are shown in fig. 9. The model seems to be able to reproduce the data (the fusion model prescriptions used in sect. 4 are valid only for meson-meson production).

Fig. 10(a) shows the distribution of the transverse correlation angle $\Delta\phi$ for the same $K^o_s\Lambda$ sample. The distribution is flat with an average

value of (97.3 ± 10.1)degrees. The ratio of the p_T's of the two V°s is plotted in fig. 10(b). The distribution has an average value of 0.47 ± 0.07. Lund model predictions agree with the data reasonably well.

6. RESULTS ON K^o_s-$\bar{\Lambda}$ AND $\Lambda\bar{\Lambda}$ CORRELATION

We have observed 14 pairs of $K^o_s\bar{\Lambda}$ and 11 pairs of $\Lambda\bar{\Lambda}$ events. These events after proper correction give rise to a cross section of (0.26 ± 0.07)mb for $K^o_s\bar{\Lambda}$ and (0.10 ± 0.03)mb for $\Lambda\bar{\Lambda}$ production. These two processes together explain the bulk of the inclusive $\bar{\Lambda}$ production. We have obtained a cross section of (0.04 ± 0.02) mb for $\Lambda\bar{\Lambda}$ production with Λ and $\bar{\Lambda}$ emitted in the backward hemisphere. At 400 GeV/c pp interactions [39] one quotes (0.12 ± 0.07) mb for $\Lambda\bar{\Lambda}$ production with Λ and $\bar{\Lambda}$ in the backward hemisphere.

The mean rapidity gap of the $K^o_s\bar{\Lambda}$ and $\Lambda\bar{\Lambda}$ samples are 0.82 ± 0.21 and 1.10 ± 0.21 respectively. The mean transverse correlation angles of the two samples are respectively (81 ± 11) and (78 ± 14)degrees.

7. SUMMARY

In this work the correlation properties between neutral strange particles have been studied in 360 GeV/c pp interactions, and longitudinal and transverse correlations have been compared with predictions of the quark fusion and Lund models.

(a) The inclusive $K^o_sK^o_s$, $K^o_s\Lambda$, $K^o_s\bar{\Lambda}$ and $\Lambda\bar{\Lambda}$ cross sections are determined to be (1.74 ± 0.18), (1.48 ± 0.17), (0.26 ± 0.07) and (0.10 ± 0.03)mb respectively. Both the $K^o_sK^o_s$ and $K^o_s\Lambda$ cross sections increase with beam energy. A large fraction of $K^o_sK^o_s$ comes from $K^{*\pm}(890)K^o_s$ and $K^{*\pm}(890)K^{*\mp}(890)$.

(b) The rapidity gap (Δy) and Feynman x gap (Δx) distributions for $K^o_sK^o_s$ peak at zero. The two K^o_s's seem to be produced in the same rapidity range with a certain degree of positive correlation. Although the quark fusion model is compatible with experiment within errors, the Lund model seems to agree with data better. The transverse

correlations in terms of $\Delta\phi$ (the angle between K_s^o and K_s^o in the transverse plane) and p_{T_1}/p_{T_2} ($p_{T_1} \leq p_{T_2}$) are equally well described by both models.

(c) The Δy, Δx, $\Delta\phi$ and p_{T_1}/p_{T_2} distributions are also studied for $K_s^o\Lambda$ production and results compared with the Lund model. There is good agreement between data and the model predictions.

REFERENCES

[1] V.V. Anisovich and V.H. Shekhter, Nucl. Phys. B55 (1973) 455; Sov. J. Nucl. Phys. 27 (1978) 567.

[2] P.V. Landshoff and J.C. Polkinghorne, Phys. Rep. 5C (1972) 1.

[3] W. Ochs, Nucl. Phys. B118 (1981) 397.

[4] E. Reya, Phys. Rep. 69C (1981) 195.

[5] S.J. Brodsky and J.F. Gunion, Phys. Rev. D17 (1978) 848.

[6] K.P. Das and R.C. Hwa, Phys. Lett. 68B (1977) 459.

[7] J.F. Gunion, Phys. Rev. D12 (1975) 1345.

[8] D. Sivers, Nucl. Phys. B106 (1976) 95.

[9] V.V. Kniazev et al., preprint IHEP 77-06, Serpukhov (1977).

[10] P.V. Chliapnikov et al., Nucl. Phys. B148 (1979) 400.

[11] Yu. V. Fisjak and E.P. Kistenev, Z. Phys. C10 (1981) 307.

[12] K. Fialkowski and W. Kittel, Rep. Prog. Phys. 46 (1983) 1283.

[13] B.L. Combridge, Nucl. Phys. B151 (1979) 429.

[14] V. Barger et al., Phys. Rev. D15 (1982) 121.

[15] A. Donnachie and P.V. Landshoff, Nucl. Phys. B112 (1976) 233.

[16] R. Moore and A. Donnachie, J. Phys. G4 (1978) 1885.

[17] A. Donnachie, Z. Phys. C4 (1980) 161.

[18] C.E. Carlson and R. Suaya, Phys. Lett. 81B (1979) 329.

[19] R. Winder and C. Michael, Nucl. Phys. B173 (1980) 59.

[20] R.P. Feynman et al., Nucl. Phys. B128 (1977) 1.

[21] S.N. Ganguli and M. Schouten, Z. Phys. C19 (1983) 83.

[22] S.N. Ganguli, Z. Phys. C21 (1983) 163.

[23] F. Ochiai et al., Z. Phys. C23 (1984) 369.

[24] D. Bertrand et al., Nucl. Phys. B128 (1977) 365.

[25] R. Harris et al., Phys. Rev. D18 (1978) 92.

[26] P.V. Chliapnikov et al., Nucl. Phys. B102 (1976) 61.

REFERENCES (Cont'd)

[27] J.L. Bailly et al., Z. Phys. C22 (1984) 119.

[28] J.L. Bailly et al., Z. Phys. C23 (1984) 205.

[29] M. Asai et al., Z. Phys. C27 (1985) 11.

[30] S. Banerjee and A. Gurtu, Bombay Note, TIFR-BC-83-7 (1983).

[31] M. Gluck et al., Z. Phys. C13 (1982) 119.

[32] T. Sjostrand, Lund preprint LUTP 82-3 (1982);
B. Andersson et al., Phys. Rep. 97 (1983) 33;
T. Sjostrand, Comp. Phys. Comm. 27 (1982) 243;
T. Sjostrand, Comp. Phys. Comm. 28 (1983) 229.

[33] C.N. Booth et al., Phys. Rev. D27 (1983) 2018.

[34] K. Jaeger et al., Phys. Rev. D11 (1975) 1756.

[35] K. Alpgard et al., Nucl. Phys. B103 (1976) 234.

[36] V.V. Ammosov et al., Nucl. Phys. B115 (1975) 269.

[37] F. LoPinto et al., Phys. Rev. D22 (1980) 573.

[38] M. Aguilar-Benitez et al., Rev. Mod. Phys. 56 (1984).

[39] R.D. Kass et al., Phys. Rev. D20 (1979) 605.

FIGURE CAPTIONS

Fig. 1 (a) Inclusive $K^o_s K^o_s$ cross section as a function of incident proton momentum.

(b) Ratio of inclusive $K^o_s K^o_s$ cross section to inclusive K^o_s cross section as a function of incident proton momentum.

Fig. 2 Semi-inclusive effective mass distribution of $K^o_s \pi^{\pm}$ system in association with a second K^o_s. The smooth solid curve is the result of the fit as described in the text.

Fig. 3 Effective mass distributions of (a) $K^o_s \pi^-$ and (b) $K^o_s \pi^+$ system where the other $K^o_s \pi^{\pm}$ system has an effective mass in the $K^*(890)$ band (0.80-1.00) GeV/c^2. The smooth curves are the results of the fit.

Fig. 4 Various kinematic distributions of the $K^o_s K^o_s$ system: (a) Feynman x variable; (b) transverse momentum squared; (c) effective mass. The smooth curves are fits as described in the text.

Fig. 5 (a) Rapidity gap; (b) Feynman x-gap distributions of the inclusive $K^o_s K^o_s$ sample. The solid circles refer to the total sample and the open circles to the events in which both K^o_s are in the backward hemisphere. The full curves are predictions of the fusion model and the dotted curves are the predictions of the Lund model.

Fig. 6 Distributions of the (a) azimuthal correlation angle $\Delta\phi$, (b) ratio of the transverse momenta p_{T_1}/p_{T_2} with $p_{T_1} \leq p_{T_2}$ for the $K^o_s K^o_s$ sample. The notation is the same as in fig. 5.

Fig. 7 Inclusive $K^o_s \Lambda$ cross section as a function of laboratory beam momentum.

Fig. 8 Various kinematic distributions of the $K^o_s \Lambda$ system: (a) Feynman x-variable; (b) transverse momentum squared; (c) effective mass. The smooth curves are results of fits as described in the text.

FIGURE CAPTIONS (Cont'd)

Fig. 9 (a) Rapidity gap; (b) Feynman x-gap distributions of the $K^o_s\Lambda$ sample where both K^o_s and Λ are emitted in the backward hemisphere. The curves are Lund model predictions.

Fig. 10 Distributions of the (a) azimuthal correlation angle $\Delta\phi$; (b) ratio of the transverse momenta p_{T_1}/p_{T_2} with $p_{T_1} \leq p_{T_2}$ for the $K^o_s\Lambda$ sample where both K^o_s and Λ are emitted in the backward hemisphere. The curves are Lund model predictions.

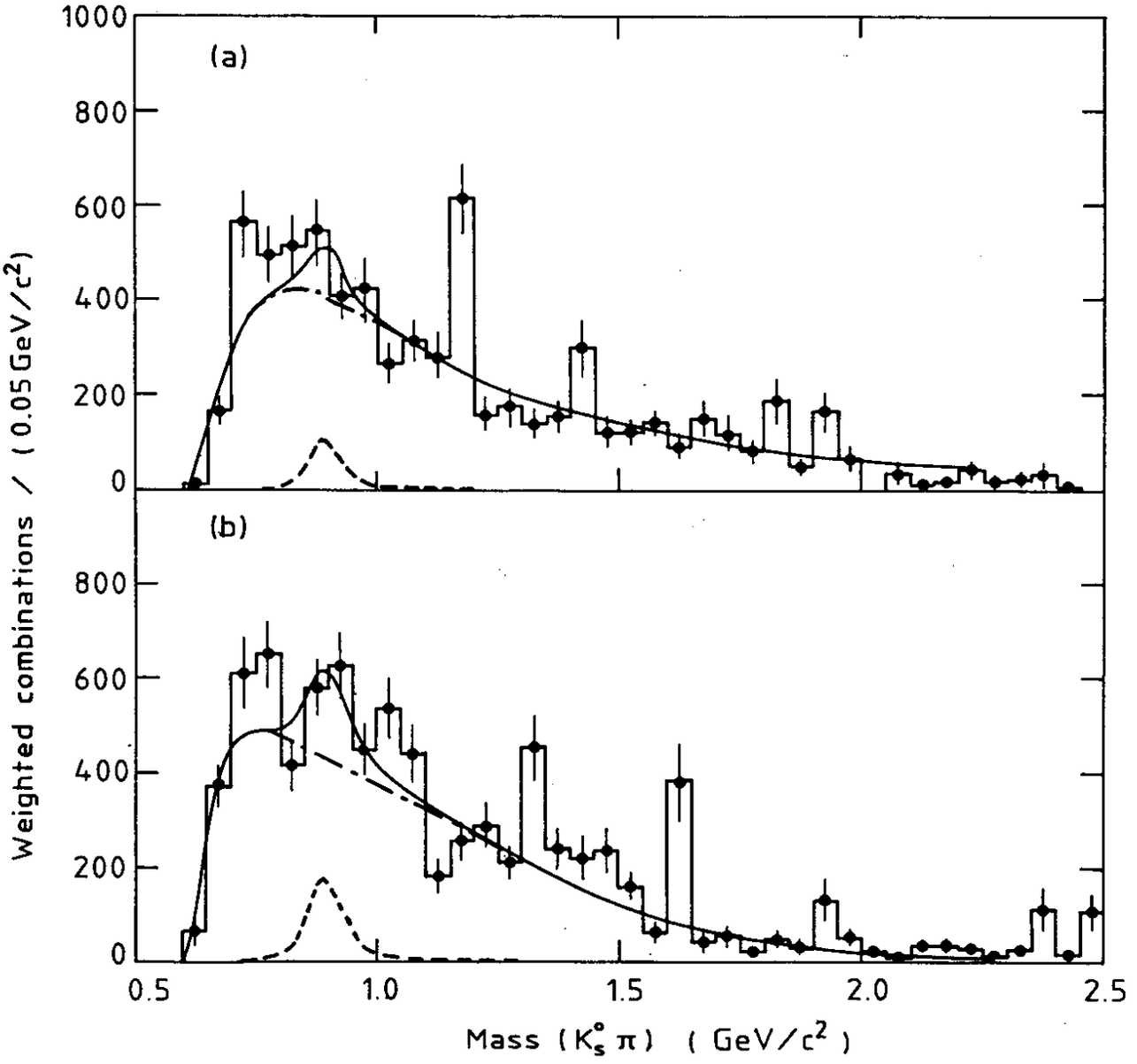
(a)
(b)
1000
800
600
400
200
0
Weighted combinations / (0.05 GeV/c²)
0.5
1.0
1.5
2.0
2.5
Mass (K°s π) (GeV/c²)

Fig. 3

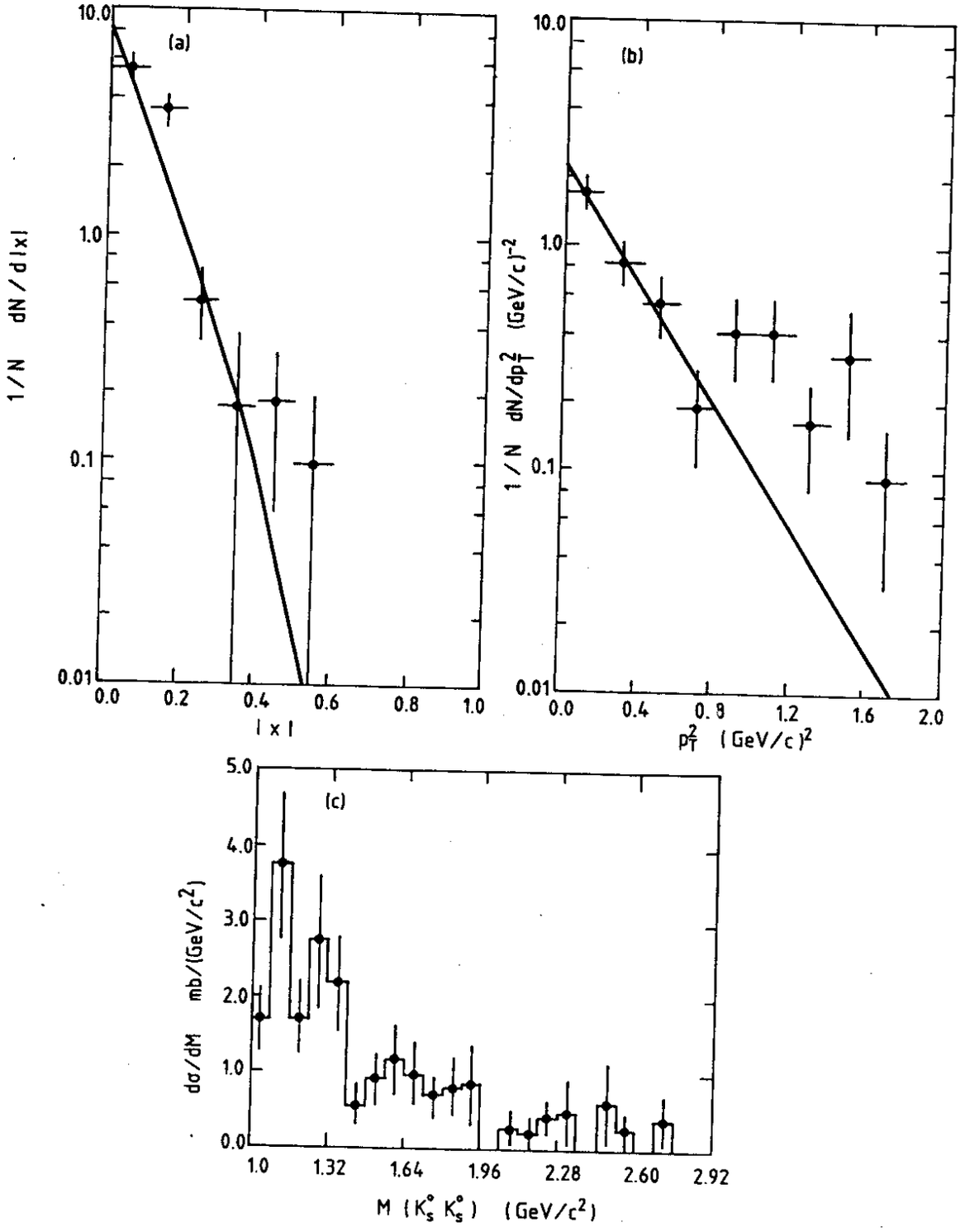
(a)
10.0
1.0
0.1
0.01
1 / N dN / d |x|
0.0
0.2
0.4
0.6
0.8
1.0
| x |
(b)
10.0
1.0
0.1
0.01
1 / N dN/dp$_T^2$ (GeV/c)$^{-2}$
0.0
0.4
0.8
1.2
1.6
2.0
p$_T^2$ (GeV/c)^2
(c)
5.0
4.0
3.0
2.0
1.0
0.0
dσ/dM mb/(GeV/c^2)
1.0
1.32
1.64
1.96
2.28
2.60
2.92
M (K$_s^o$ K$_s^o$) (GeV/c^2)

Fig. 4

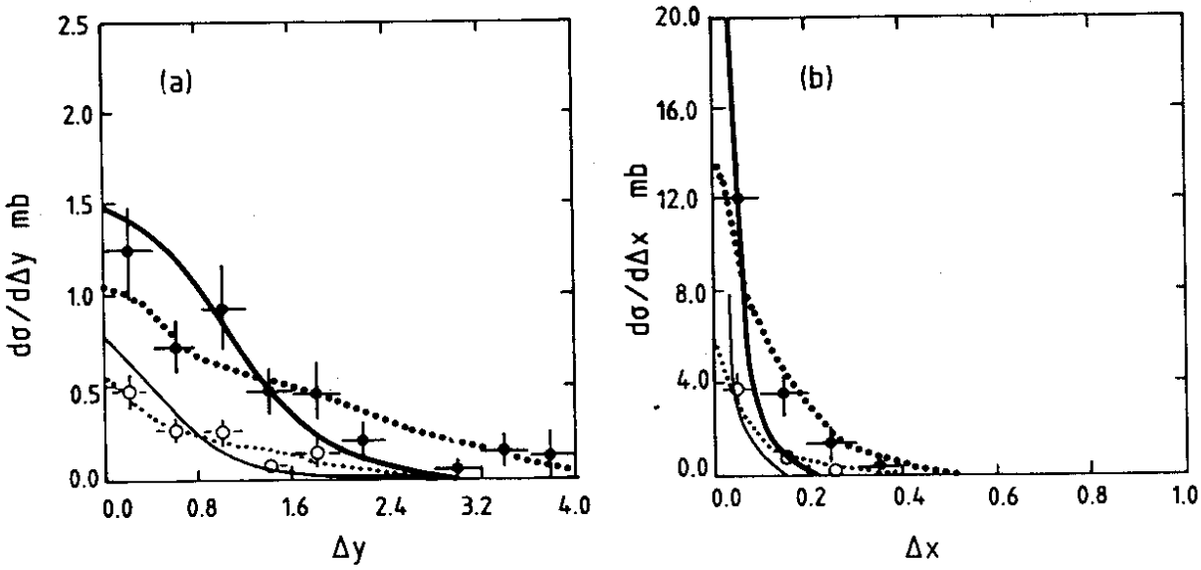
(a)
(b)
dσ/dΔy mb
dσ/dΔx mb
Δy
Δx
2.5
2.0
1.5
1.0
0.5
0.0
0.8
1.6
2.4
3.2
4.0
20.0
16.0
12.0
8.0
4.0
0.2
0.4
0.6

Fig. 5

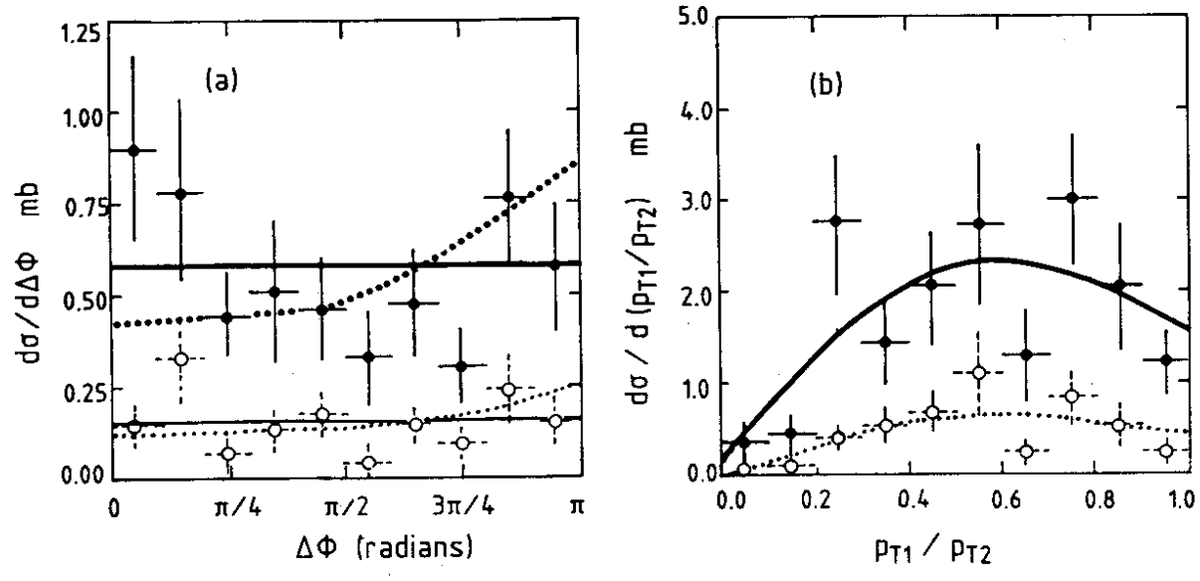
(a)
(b)
dσ/dΔΦ mb
dσ / d (pT1/pT2) mb
ΔΦ (radians)
pT1 / pT2
1.25
1.00
0.75
0.50
0.25
0.00
0
π/4
π/2
3π/4
π
5.0
4.0
3.0
2.0
1.0
0.0
0.2
0.4
0.6
0.8

Fig. 6

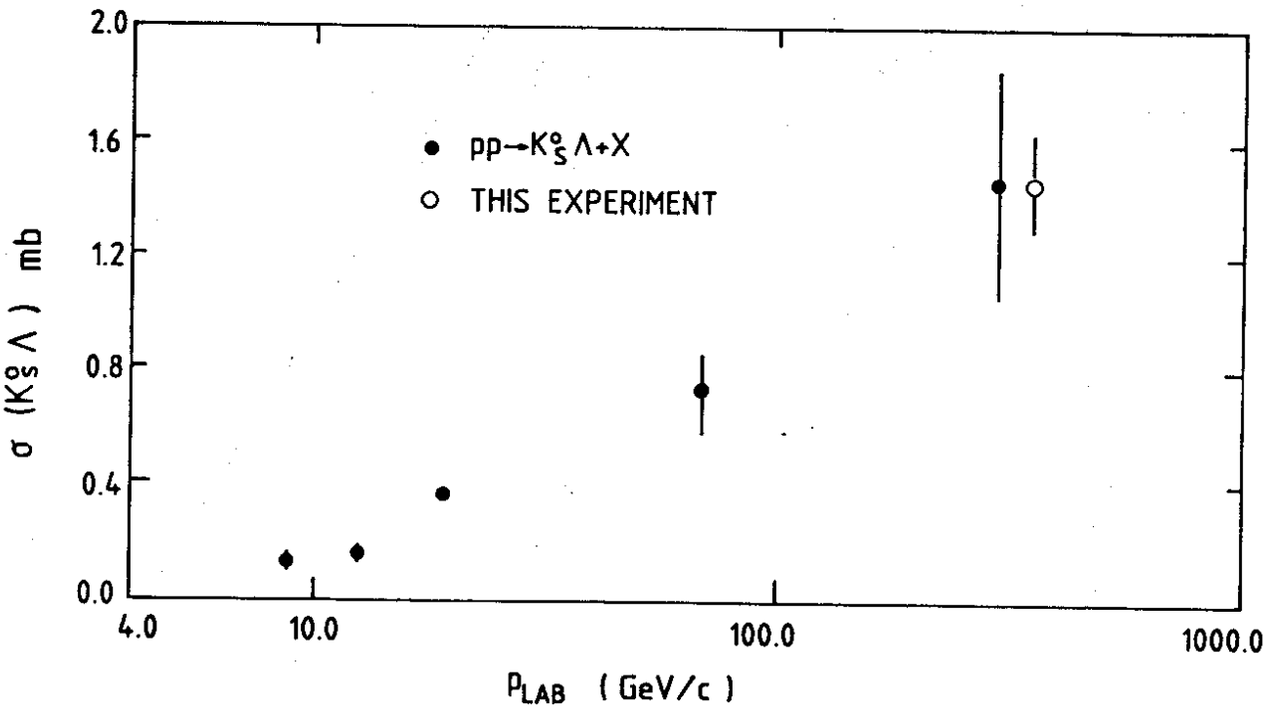
2.0
1.6
1.2
0.8
0.4
0.0
σ (K°S Λ) mb
pp→K°S Λ+X
THIS EXPERIMENT
4.0
10.0
100.0
1000.0
PLAB (GeV/c)

Fig. 7

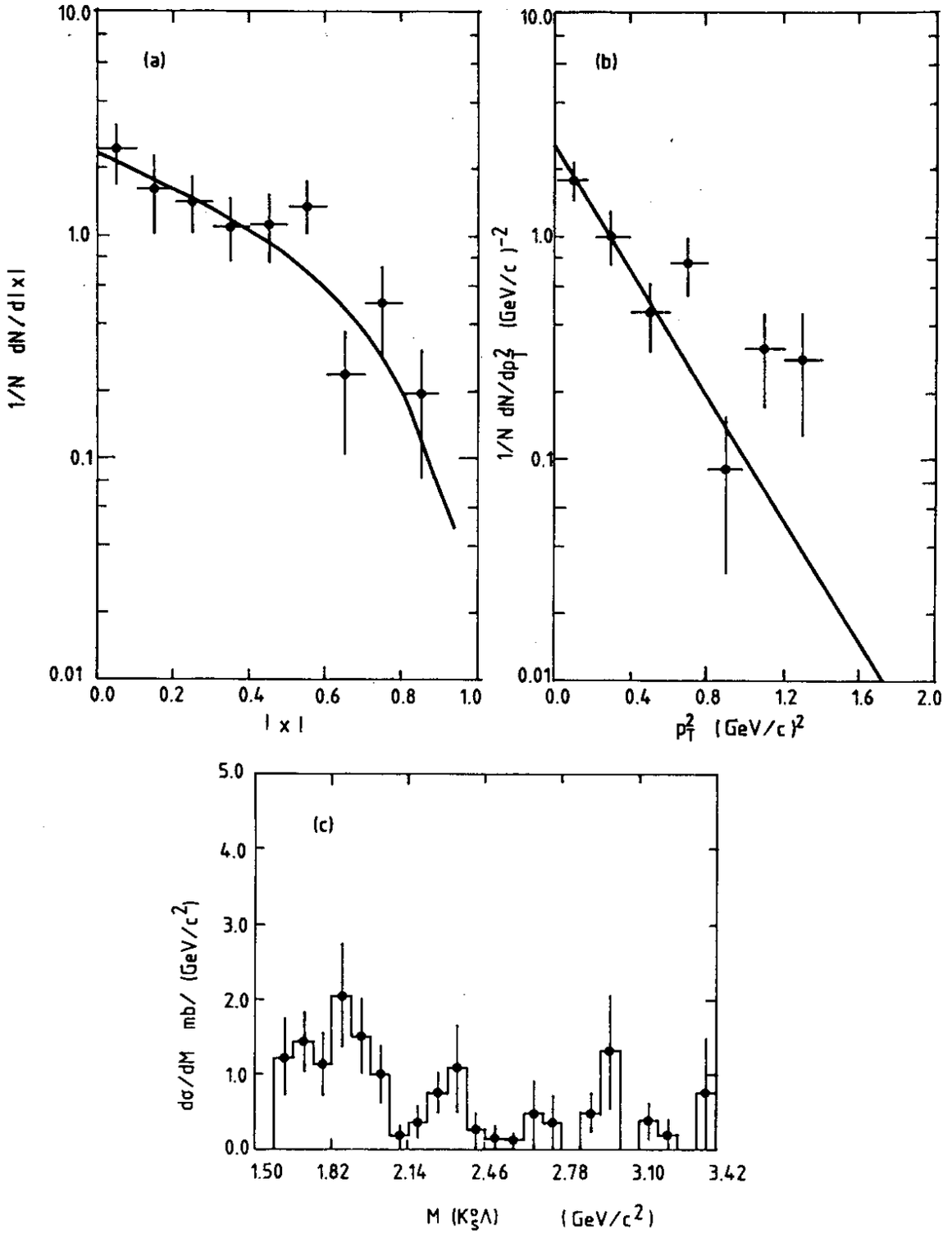
(a)
1/N dN/d|x|
|x|
(b)
1/N dN/dp$_T^2$ (GeV/c)$^{-2}$
p$_T^2$ (GeV/c)^2
(c)
dσ/dM mb/ (GeV/c^2)
M (K^o_SΛ) (GeV/c^2)

Fig. 8

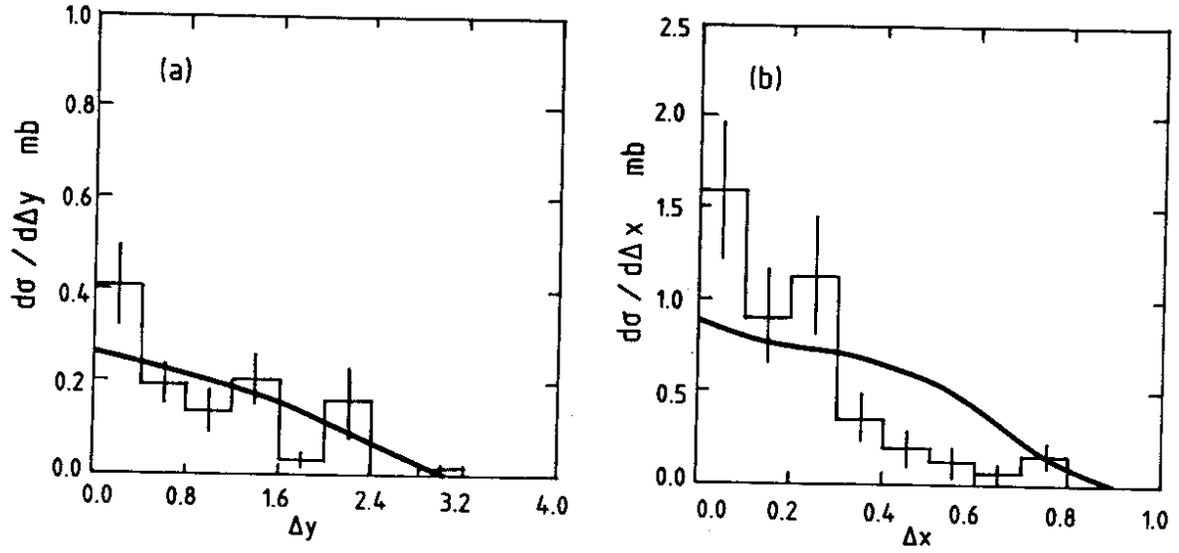
(a)
dσ / dΔy mb
Δy
(b)
dσ / dΔx mb
Δx

Fig. 9

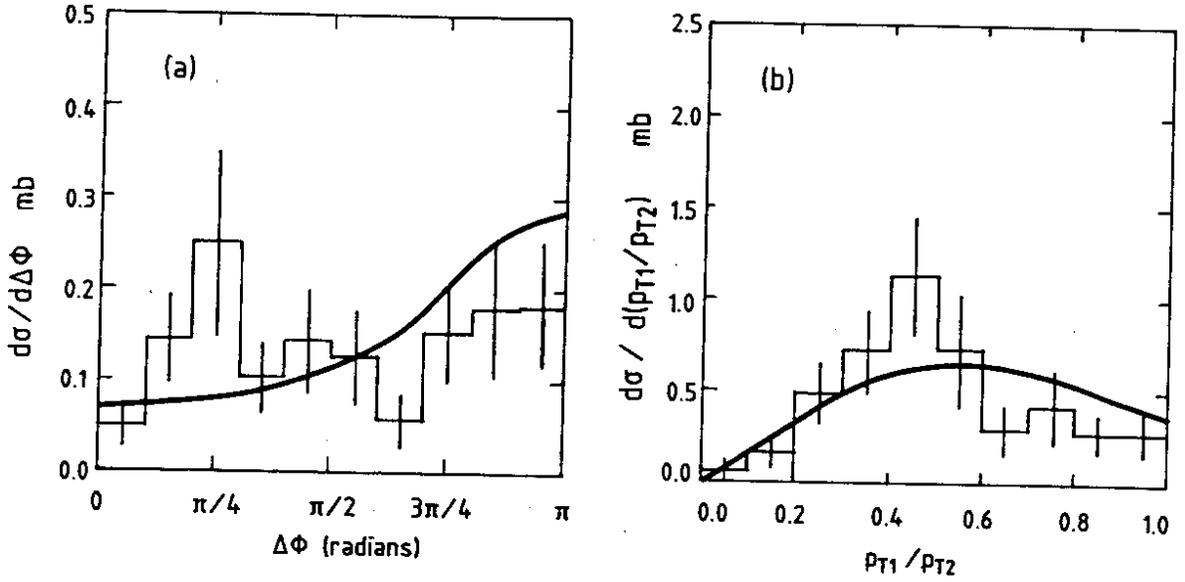
(a)
dσ/dΔΦ mb
ΔΦ (radians)
(b)
dσ / d(pT1/pT2) mb
pT1 /pT2

Fig. 10